SPS KICKER IMPEDANCE MEASUREMENT AND SIMULATION

F. Caspers, CERN, Geneva, Switzerland

Abstract

The beam coupling impedance of several SPS kickers has been investigated by means of the classical coaxial wire method as well as using simulations with the HFSS code and heating caused by the beam. The results and interpretation of wire method as well as numerical simulations are discussed and possible implications for near and medium term future are taken into consideration.

1 INTRODUCTION

In the context of increasing demands for beams circulating in the SPS (LHC injection, Grand Sasso neutrino project) the impedance of this machine is an important issue. There are essentially two aspects of kicker related impedances, namely heating of the kicker and beam stability. Heating is caused in the present case by spectral components, which are integer multiples of 200 MHz (bunch spacing 5 ns) and have to be considered up to about 1 GHz for currently used bunch length. These spectral components interact with the real part of the kicker impedance and can lead to a clearly measurable (temperature difference more than $10\,^{\circ}$C) heating of the kicker modules. For beam stability issues, both the real and imaginary part are relevant, even for frequencies much smaller than 200 MHz. A reasonably precise impedance estimate, based on coaxial wire data, numerical simulations and analytical models will help to identify and predict stability problems. This knowledge can also be used to implement constructive measures such as the installation of rf-bypasses to reduce the impedance in critical regions. In the following we are considering two types of kicker installed in the SPS. Cross sections of the fast extraction kicker magnet (MKE) and the inflector kicker magnet (MKP) are shown in Fig. 1.

2 MODELS FOR CALCULATION OF LONGITUDINAL COUPLING IMPEDANCE

For the numerical and analytical calculations we used four models as shown in Fig. 2.

Model 1 is a metal tube with inner radius d, which is homogeneously filled with a hollow ferrite cylinder of outer radius d and inner radius b. The beam is in the center at $r = 0$. The length in axial direction is infinite for analytical calculations.

Model 2 is a metal tube with square cross section ($|x| < a, |y| < b$) and two ferrite slabs ($|x| < a, b < |y| < d$). The image current can find a metallic by-passes left and right ($|x| > a$). The length in axial direction is infinite for analytical calculations.

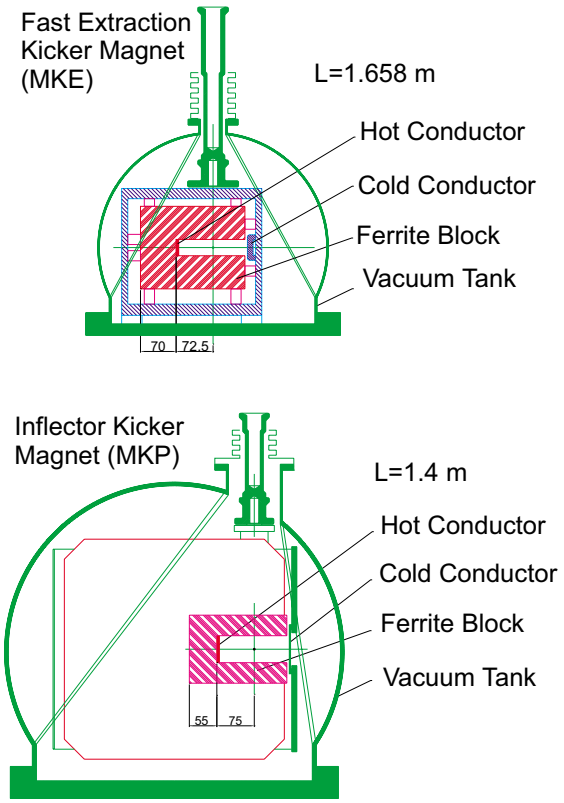

Figure 1: Cross sections of the SPS MKE and MKP kicker magnets.

Model 3 is closer to the cross section of the MKE kicker in particular with respect to the "hot" and "cold" conductor.

Model 4 is similar to Model 3 but takes into account also the vacuum tank surrounding the kicker module.

2.1 *Model 1*

Analytical Calculation with Beam The analytical formula of the longitudinal coupling impedance per unit length Z/L is derived using the field matching technique [1]:

$$\frac{Z}{L} = j\frac{Z_0}{2\pi b}\left[FH\frac{k\epsilon_r}{k_r} - \frac{kb}{2}\right]^{-1},$$

$$FH = \frac{H_0^{(1)}(k_r d)H_1^{(2)}(k_r b) - H_0^{(2)}(k_r d)H_1^{(1)}(k_r b)}{H_0^{(1)}(k_r d)H_0^{(2)}(k_r b) - H_0^{(2)}(k_r d)H_0^{(1)}(k_r b)}, \quad (1)$$

where ϵ_r, μ_r, Z_0, k, k_r, H are the relative permittivity, the relative permeability, impedance in vacuum ($Z_0 = c\mu_0$), ω/c, $k\sqrt{\epsilon_r\mu_r - 1}$, and the Hankel function, respectively. The solid line in Fig. 3 shows the result, where we assumed

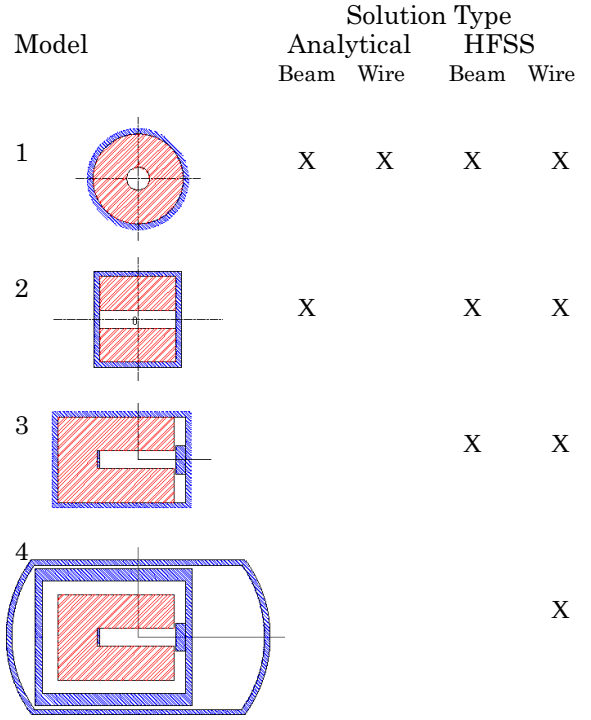

Figure 2: Simplified kicker models. All analytical solutions are two dimensional, and have infinite length. All numerical models have finite lengths.

$b = 20$ mm, $d = 80$ mm, and the length of the ferrite block l_F is 1658 mm.

HFSS Simulation with Beam We used 1/36 model (i.e. a sector of $10°$) for the simulation because this geometry has axial symmetry. Since HFSS has an option to assign sinusoidal time dependent currents on planar surfaces, we used this to simulate the beam [1, 2]. Current sources of 2 cm length are aligned on the beam axis. Thus, the phase difference between adjacent currents is 2 cm / $\lambda \times 360°$. The length in axial direction is now finite and equal to 1 m. The circle symbols in Fig. 3 show the results, which agree with the analytical calculation (solid lines).

Analytical Calculation with Wire There are several coupling impedance formulae available for coaxial wire measurement.

The formula given by Hahn and Pedersen for a single lumped impedance model is [3]:

$$Z_{HP} = 2Z_c \frac{S_{21ref} - S_{21DUT}}{S_{21DUT}}, \tag{2}$$

where S_{21DUT} is the transmission coefficient of the device under test (DUT). The transmission coefficient of the reference S_{21ref} is $\exp(-j\omega l/c)$, where l is the length of the DUT. The characteristic impedance Z_c is given in [6] as,

$$Z_c = \frac{Z_0}{2\pi} \log\left(\frac{b}{a}\right), \tag{3}$$

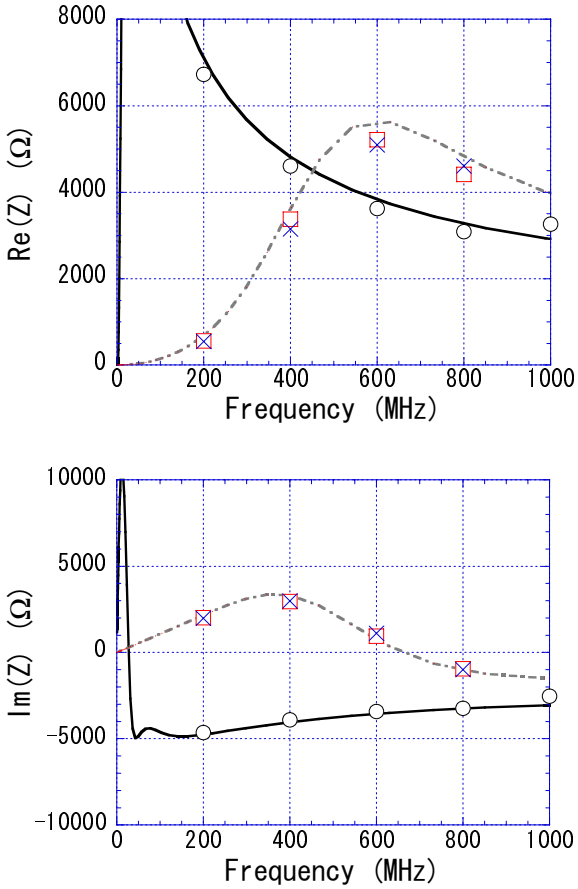

Figure 3: Longitudinal coupling impedance with beam for the SPS MKE kicker by analytical calculation and HFSS simulation. The circle, rectangular, and "×" symbols are the HFSS (beam) results for Model 1, 2, and 3, respectively. The solid line shows the analytical result for Model 1. The dashed line shows the analytical result for Model 2.

where a is the wire radius.

For distributed impedance systems like our case, often the "standard" log (log in miniscules = standard) formula is used in the coaxial wire measurement [6]:

$$Z_{log} = -2Z_c \log\left(\frac{S_{21DUT}}{S_{21ref}}\right). \tag{4}$$

If the DUT impedance exceeds significantly the value of Z_c, then the "improved" LOG (LOG in majuscules = improved) formula [7, 8] gives better results at least for the real part:

$$Z_{LOG} = Z_{log}\left[1 + \frac{jc}{2\omega l_F} \log\left(\frac{S_{21DUT}}{S_{21ref}}\right)\right], \tag{5}$$

where l_F is the length of the ferrite block in the DUT.

The transmission coefficient S_{21DUT} in our case is $\exp(-\gamma l)$, where γ is the attenuation constant. Thus the above formulae become

$$Z_{HP} = 2Z_c[\exp\{(\gamma - j\omega/c)l_F\} - 1],$$

$$Z_{log} = 2Z_c l_F \left(\gamma - j\frac{\omega}{c}\right),$$
$$Z_{LOG} = -jZ_c l_F \frac{c}{\omega}\left(\gamma^2 + \frac{\omega^2}{c^2}\right). \quad (6)$$

They go to a same value when the wire radius a goes to zero.

The attenuation constant γ can be calculated by the field matching technique [1]. The solid line in Fig. 4 shows the calculated longitudinal coupling impedance with wire.

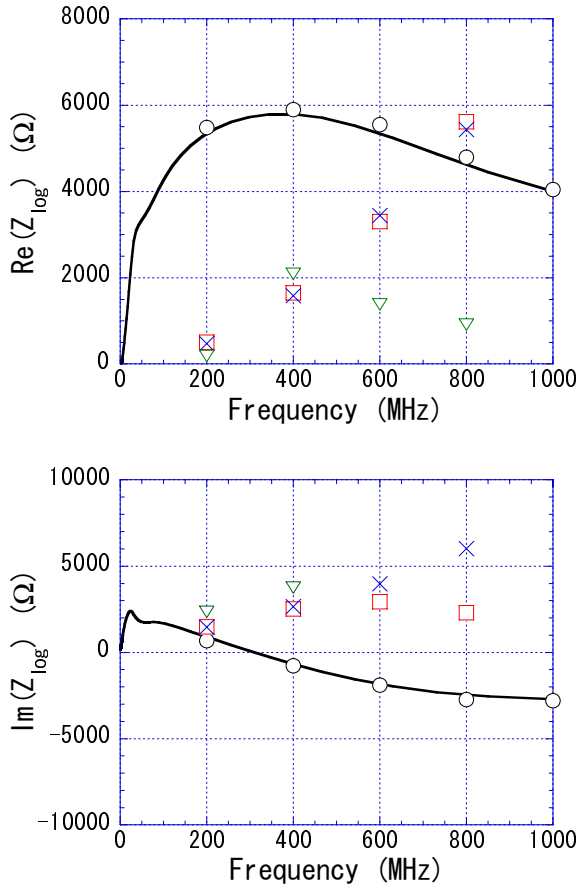

Figure 4: Longitudinal coupling impedance with wire for the SPS MKE kicker by analytical calculation and HFSS (wire) simulation. The circle, rectangular, "×", and triangle symbols are the HFSS (wire) results for Model 1, 2, 3, and 4, respectively. The solid line shows the analytical result for Model 1.

Figures 5, 6 show the result as a function of the wire radius. For Model 1, the (improved) LOG formula looks much better.

HFSS Simulation with Wire The axial length of the ferrite is assumed to be 1 m here. We add two beampipe sections of 5 cm length, 2 cm radius on both sides in order to have regular TEM modes at both ports. The radius of the wire is 1 mm. The characteristic impedance Z_c of the coaxial beampipe is $Z_0/(2\pi)\log(20/1) = 180\ \Omega$.

The circle symbols in Fig. 4 show the result with

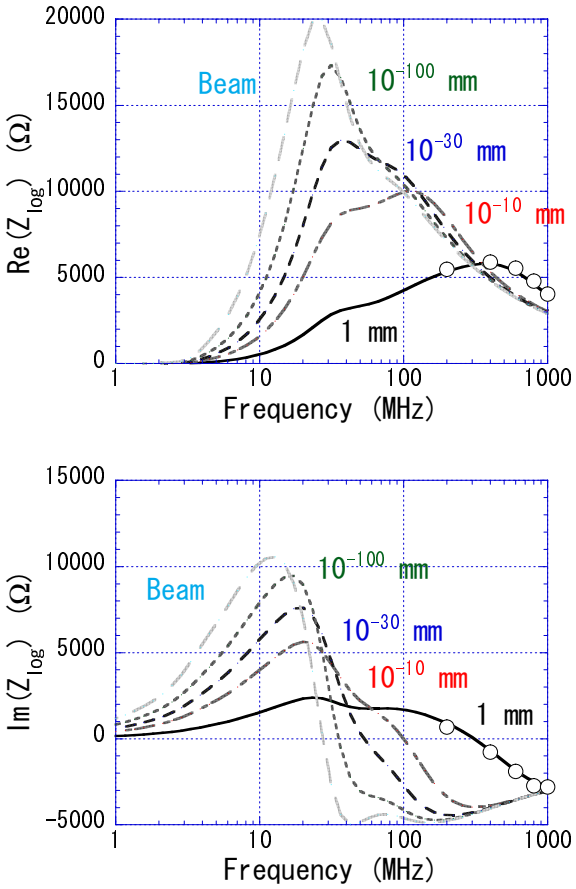

Figure 5: Longitudinal coupling impedance as a function of wire radius for Model 1 (the (standard) log formula (4)).

HFSS(wire). The result agrees well with the analytical calculation (solid lines).

2.2 *Model 2*

As compared with the measurement (Section 3), Model 1 gives much larger impedance below 200 MHz. This may be because we neglected the metal electrode plates at either side. In the kicker at lower frequency, the electromagnetic field should be strongly deformed so that most of the image current passes via the electrode plates. This reduces the impedance at low frequency. Thus, electrodes were added at either side in the Model 2, and we deformed the ferrite block in order to calculate the impedance analytically.

Analytical Calculation with Beam The analytical formula is given in [1] as

$$\frac{Z}{L} = j\frac{Z_0}{2a}\sum_{n=0}^{\infty}\left[FX + FY - \frac{k}{k_{xn}}sh\ ch\right]^{-1},$$
$$FX = \frac{k_{xn}}{k}\frac{(1+\epsilon_r\mu_r)sh\ ch}{\epsilon_r\mu_r - 1},$$
$$FY = \frac{k_{yn}}{k}\frac{(\mu_r sh^2 tn - \epsilon_r ch^2 ct)}{\epsilon_r\mu_r - 1}, \quad (7)$$

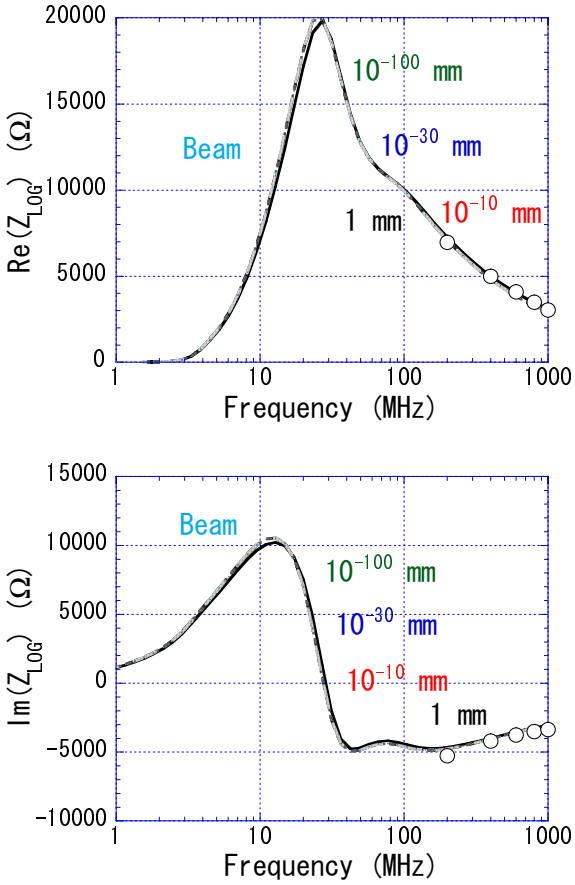

Figure 6: Longitudinal coupling impedance as a function of wire radius for Model 1 (the (improved) LOG formula (5)).

where wave numbers k_{xn} and k_{yn} are $(2n+1)\pi/(2a)$ and $\sqrt{(\epsilon_r\mu_r-1)k^2-k_{xn}^2}$, respectively. The parameters sh, ch, tn, and ct are $\sinh(k_{xn}b)$, $\cosh(k_{xn}b)$, $\tan(k_{yn}(b-d))$, and $\cot(k_{yn}(b-d))$, respectively.

The result is shown as dashed lines in Fig. 3. Below 200 MHz, the result agrees with the measurement (Section 3). But at higher frequencies, the real part of the impedance is 2–3 times higher than obtained from the measurements.

HFSS Simulation with Beam Since this geometry is symmetric with respect to the $x = 0$ and $y = 0$ planes, we use 1/4 model (i.e. a sector of $90°$) to carry out the simulation. Thus we need much more volume to simulate Model 2 as compared to Model 1. Since the number of tetrahedras should not exceed about 50000 due to the computer resource problem at CERN, we could not make the mesh size small enough. We used the manual mesh option in HFSS in order to get a mesh size smaller than 10 mm, which is still not enough. For further volume reduction we diminished the axial length from 1 m to 50 cm.

The rectangular symbols in Fig. 3 show the result. The data agree with the analytical calculation (dashed lines).

HFSS Simulation with Wire In the HFSS (wire) simulation of this model, the axial length of the ferrite is 1 m. Two circular beampipes of 20 mm radius, 50 mm length, are added on either sides. The radius of the wire is 1 mm.

The rectangular symbols in Fig. 4 show the result. By comparing the result with the measurement (Section 3), we see that they agree well at 200 MHz. At 400 MHz, the real part of the impedance from the measurement is 1800 Ω, our result is 1600 Ω, thus the real parts agree well. But the imaginary part by the measurement is already considerably larger than the numerical result.

For 600 MHz, the real part of the impedance by the measurement is about twice or three times smaller than our result. The imaginary part by the measurement is much larger than the numerical result.

2.3 *Model 3*

The discrepancy between the result of the measurement and of the HFSS simulation of Model 2 may be due to the following two reasons:

- In reality, the side plates are not like Model 2.
- The ferrite block is surrounded by the vacuum tank. Some amount of electromagnetic energy travels through the space between the ferrite and and vacuum tank. This can reduce the impedance seen by the coaxial wire method at high frequencies.

To check the first point, Model 3 is studied.

Since the analytical calculation of the impedance is very complicated, we decided to carry out HFSS (beam, wire) simulations only.

HFSS Simulation with Beam The "×" symbols in Fig. 3 show the result of HFSS (beam) simulation. The value is almost the same as that of Model 2.

HFSS Simulation with Wire We added coaxial beampipes of 20 mm radius on both sides, and calculated the scattering parameters with HFSS (wire). The radius of the wire is 1 mm. Since the geometry is symmetric with respect to the $y = 0$ plane, we used 1/2 geometry (i.e. a sector of $180°$). The rectangular symbols in Fig. 4 show the longitudinal coupling impedance with wire. The behavior is a bit different from Model 2. This may be because:

- There are errors in the simulation.
- Some waveguide mode resonances change the phase and amplitude of S_{21}.

2.4 *Model 4*

Since Model 2 or Model 3 did not reproduce the measurement by the coaxial wire method, we pursue the following reasoning given in the previous subsection; the cavity mode resonances change the phase and amplitude of S_{21}.

To see the effect of this, we input an almost realistic geometry to HFSS and simulated the coaxial wire method. Since the total length of the ferrite is so long ($l_F = 1.658$ m), the mesh size is large and consequently the error is big.

HFSS Simulation with Wire The triangle symbols in Fig. 4 show the result.

Figure 7 shows the electric field on $y = 0$ plane at 600 MHz. It can be observed that the waves around the wire disappear at certain distance, whereas the small by-passing waves between the ferrite block and the vacuum tank join at the exit of the kicker. This phenomenon may give larger magnitude of S_{21} than one expects in the theory of the log formulae, and the resulting coupling impedance by the formula (4) should be smaller than the reality. The by-passing waves also change the phase of S_{21}, which results in the unexpected behavior of the imaginary part of the coupling impedance above 400 MHz. At this point around 400 MHz, the model assumed breaks down as we have coupling via cavity modes.

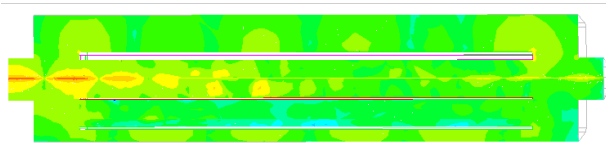

Figure 7: Electric field on the y = 0 plane at 600 MHz. The signal travels from left to right. The waves around the wire attenuate quickly, and disappear at a certain distance. Some waves transmit via the space between ferrite and vacuum tank, and join at the exit of the kicker.

3 RESULTS AND OBSERVATION OF WIRE MEASUREMENT DATA

Using the standard single wire measurement technique a number of transmission measurements were carried out on the SPS MKE kicker [6]. For practical reasons we used flat flanges at the MKE kicker beam pipe port (no conical transitions) and the diameter of the thin wire was 0.4 mm. In order to improve the matching of this wire (seen from inside the tank with respect to the 50 Ω coaxial cable) resistors were installed near either flange of the tank. The ohmic value R of these low inductance carbon resistors is simply determined by the relation: R = Z_c - 50 Ω. The approximate characteristic impedance Z_c of a thin wire in the ferrite loaded structure (Fig. 1) is determined assuming the model of a wire between two parallel conducting plates by using the relation

$$Z_c = 60 \ln[1.27 \frac{D}{d}] \quad (8)$$

For the vertical aperture D = 32 mm (horizontal aperture is 140 mm) and the wire diameter d = 0.4 mm the value of characteristic impedance Z_c is about 270 Ω.

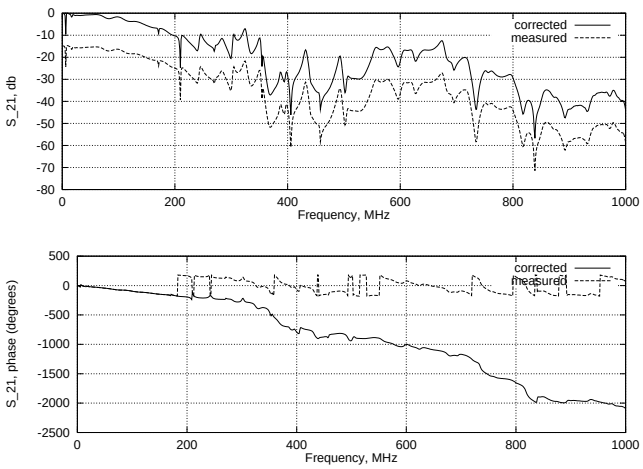

Figure 8: Corrected S-parameters for the MKE kicker: the losses from the matching resistors are taken into account, and the phase ambiguity related 360° jumps are removed.

The raw data were obtained using the HP-8753D network analyzer. In each case a cable calibration (response calibration) has been repeated and each measurement contains 801 points. The geometrical length of the kicker between the coaxial connectors was accurately measured. This length ($l = 2.2253$ m) has been taken into account via the electrical delay correction function in the network analyzer and was subtracted in the phase display.

Correction procedures were subsequently applied on both amplitude and phase data. For the amplitude (modulus) of S_{21} (S_{21} = S_{12}) we had to substract the losses attributed to the matching resistor, which were simply obtained by taking the attenuation values at the lowest frequency point (around 100 kHz to 1 MHz, depending on the frequency span used). This correction amounts approximately to 15 dB.

For the phase plots we had to remove the network analyzer display related phase ambiguities of 360°, and the procedure is most evident from Fig. 8. Note that all the resonances lead to fast phase variations vs. frequency. They may coincide and be mistaken for 360° phase jumps attributed to the network analyzer. This procedure was not applied for frequencies beyond 1 GHz since the interpretation of that data would be too questionable.

Finally, the corrected S-paramaters were plugged into Eqs. (4) and (5). The results of these calculations are shown in Figs. 9 and 10.

It should be noticed that applying the (improved) LOG formula (5) which returns a significantly higher real part as compared to the (standard) log formula when the measued S-parameters show more than about 10 dB attenuation, can also lead to surprises. For example consider the negative real part in Fig. 9 around 7 MHz. This is of course an unphysical result which may occur for certain "forbidden" ranges of amplitude and phase of the measured S-parameter. These ranges are dependent on the rel-

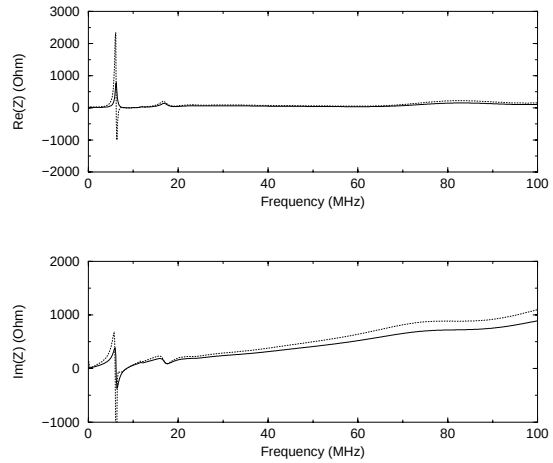

Figure 9: Impedances of the MKE kicker evaluated from the corrected values of amplitude and phase of S_{21}. The solid and dotted lines show the results by the (standard) log formula and the (improved) LOG formula, respectively.

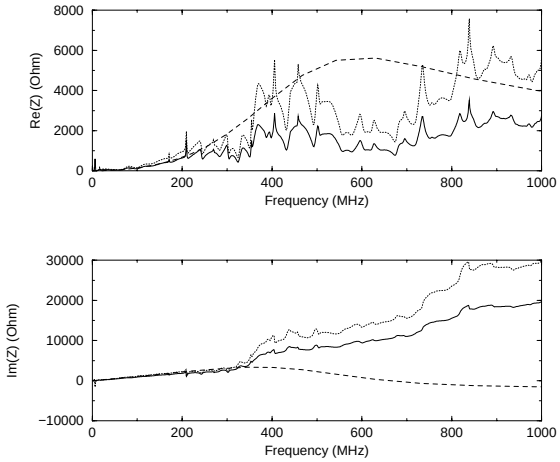

Figure 10: Impedances of the MKE kicker evaluated from the corrected values of amplitude and phase of S_{21}. The solid and dotted lines show the results by the (standard) log formula and the (improved) LOG formula, respectively. The dashed line represents the analytical calculation of Model 2.

ative electrical length of the DUT and become in particular visible when using the (improved) LOG formula for short (as compared to the free space wavelength) DUTs. This effect is not caused by an incorrect S-parameter measurement, but simply by the fact that the physical reality does not correspond to what is assumed in the model (e.g. physical reality = lossy line + resonator; mode = lossy line only.) Related aspects are also treated in [4] and ranges of validity of the different formulae have been investigated graphically in [5]. Negative real parts may occur as well when applying the lumped element model where this not appropriate, even if the amplitude of S_{21} is smaller than

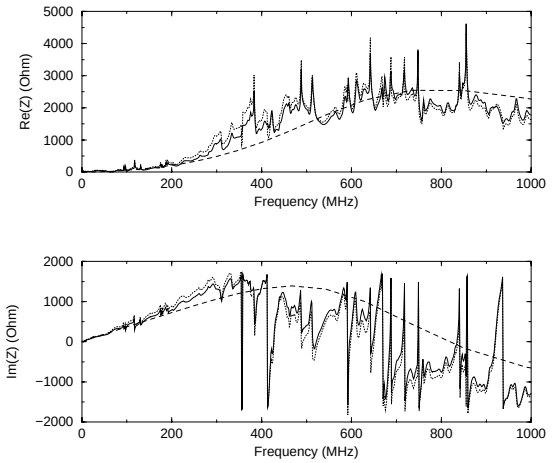

Figure 11: Impedances of the MKP kicker evaluated from the corrected values of amplitude and phase of S_{21}. The solid and dotted lines show the results by the (standard) log formula and the (improved) LOG formula, respectively. The dashed line represents the analytical calculation of Model 2.

unity. The correlation of the real part of the impedance with results obtained from different numerical and analytical calculations given in [1] as well as heating data (towards the end of this note) leads to the following assumption: The real part (the (improved) LOG formula) shown in Fig. 10 is reasonably close (within a factor of about 2) to what we may consider the true real part of the longitudinal impedanace (at least up to 400-500 MHz). As for the imaginary part, using a similar reasoning this may also be acceptable to about 400-500 MHz. The imaginary part of the MKE kicker impedance, evaluated from the measured S-parameters, exhibits rather large values for frequencies higher than about 400 MHz. If these values were considered to be true, they would violate the condition that real and imaginary part of the impedance for this kind of structures are mutually dependent and to a certain extent can be deduced from each other. The frequency limit, given here is deduced from numerical simulations described in [1].

We have noticed several high-Q resonances which are probably modified cavity resonances between the tank and the kicker module. This kicker module does not have (yet) short direct connections to the end of the tank and the cold conductor in the ferrite module. Thus cavity resonances are easily excited by the beam passing through the gaps on each side of the ferrite module.

Figure 11 shows the result for the MKP kicker. The hypothesis that the impedance seen by the wire becomes considerably reduced or limited by cavity modes by-passing the kicker block, is also supported by the strange phase response in that region for the MKE kicker. However for the MKP kicker, the by-passing effect looks to be much less pronounced, as the true impedance is smaller (larger gap, model calculation) as for the MKE.

4 BEAM SPECTRUM DURING THE FIXED TARGET CYCLE IN THE SPS

The beam spectrum of M identical bunches separated in time by T_0/h can be written in the form [6]

$$I_n = I_0 \frac{\sin(\pi\alpha_n)}{\pi\alpha_n(1-\alpha_n^2)} \frac{\sin(\pi n M/h)}{M\sin(\pi n/h)} e^{j\pi(M-1)n/h}, \quad (9)$$

where T_0, h, α_n, and I_0 are the revolution time, the harmonic number, $n\tau/T_0$, and the average beam current, respectively. Here, we have assumed the bunch current is proportional to

$$\cos^2(\pi t/\tau), -\tau/2 < t < \tau/2. \quad (10)$$

In the case of the fixed target proton beam in the SPS, $M/h = 10/11$ of the ring are filled with 5 ns spaced bunches. For a uniform distribution of bunches over the ring, the beam spectrum contains lines only at multiples of the bunch spacing frequency $h/T_0 = 200$ MHz. The existence of the gap gives additional lines around the harmonics of 200 MHz.

During the acceleration cycle, the beam spectrum is varying due to bunch length and particle distribution changes. The last happens for a high intensity beam as a result of longitudinal instabilities.

Assuming that particle distribution and longitudinal emittance stay constant during the cycle, the bunch length changes with time according to the curve shown in Fig. 12. The variation during the cycle of the RMS beam spectrum

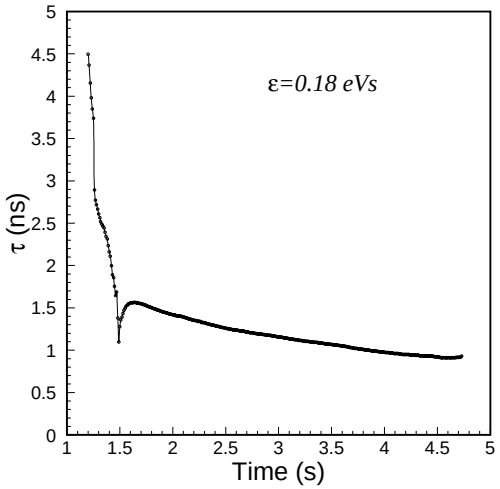

Figure 12: Bunch length for low intensity beam during SPS fixed target proton cycle in normal operation.

components

$$I_n^{rms} = \sqrt{2} I_n \quad (11)$$

is shown in Fig. 13 for multiples of RF harmonics $k = h, 2h, 3h...$ and for a total beam intensity in the ring of 10^{13}

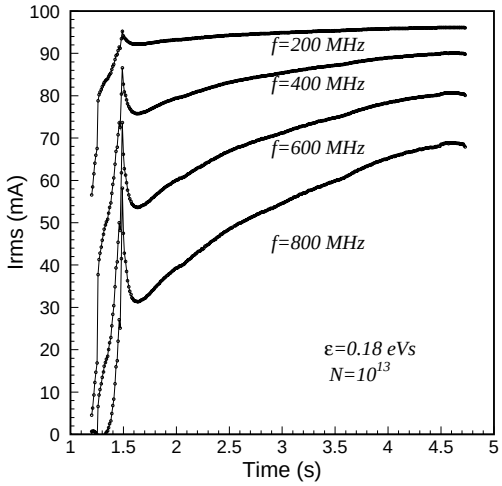

Figure 13: Beam spectrum components during SPS fixed target cycle in normal operation for beam intensity 10^{13} [6].

n	Freq. (MHz)	$\lvert I_{nh}/I_0\rvert$ t = 1.5 s	$\lvert I_{nh}/I_0\rvert$ t = 4 s	$\overline{\lvert I_{nh}/I_0\rvert}$	$\overline{\lvert I_{nh}/I_0\rvert}_c$
1	200	0.90	0.93	0.915	0.912
2	400	0.59	0.67	0.63	0.67
3	600	0.38	0.44	0.41	0.46
4	800	0.22	0.26	0.24	0.28
5	1000	0.1	0.093	0.1	0.13

Table 1: Beam spectra of the SPS at $I_0 = 132$ mA. The variable $\overline{\lvert I_{nh}/I_0\rvert}_c$ is the amplitude with the correction of cable loss.

($I_0 = 69.4$ mA). However this is valid only for a beam with total intensity at or below 10^{13}, [11]. For higher intensity beams, the bunch length does not decrease after transition crossing as is shown in Fig.12, due to continuous emittance blow-up. For the highest total intensities reached in the SPS till now (4.7×10^{13}) during normal operation cycle, the longitudinal emittance increases by a factor 10 and the effective bunch length τ corresponding to the particle distribution (Eq. (10)) is about 3 ns. Table 1 shows the bunch spectra of the SPS when $I_0 = 132$ mA.

5 COMPARISON OF POWER DISSIPATION ESTIMATES AND HEATING CAUSED BY THE SPS BEAM

The power dissipated in the kicker can be calculated with the following equation [6]:

$$P = \eta |I_0|^2 \sum_{n=-\infty}^{\infty} \mathrm{Re}(Z(n\omega_0)) |I_n/I_0|^2, \quad (12)$$

n	Freq. (MHz)	Re(Z) (Ω) Model 1	Model 2	Wire meas. log	Wire meas. LOG
0	0	0	0	0	0
1	200	7090	680	640	950
2	400	4820	3611	1750	3500
3	600	3842	5664	1350	2490
4	800	3280	4961	1870	3710
5	1000	2918	3971	2740	5610

Table 2: Real part of the longitudinal coupling impedances of Model 1, Model2, coaxial wire measurement(the (standard) log and the (improved) LOG formulae).

where η is the duty factor. Now we assume the impedance Z is broadband, and add the contributions of the sidebands

$$\sum_{n=0}^{h-1} \left| \frac{\sin(\pi n M/h)}{M \sin(\pi n/h)} \right|^2 = \frac{h}{M}.$$

Thus the power is

$$P \simeq 2\eta |I_0|^2 \frac{h}{M} \sum_{n=1}^{5} \mathrm{Re}(Z(nh\omega_0))|I_{nh}/I_0|^2. \qquad (13)$$

We apply this formula to the SPS MKE kicker. There was a measurement at I_0 = 132 mA, and the measured power is 60 W [12]. Real parts of the longitudinal coupling impedances of Model 1, Model 2, and coaxial wire measurement (the (standard) log formula, the (improved) LOG formula) are shown in Table 2. The power is

$$P = \begin{cases} 58 \sim 86\ W, & \text{Model 1} \\ 36\ W, & \text{Model 2} \\ 17\ W, & \text{Wire meas., log formula} \\ 30\ W, & \text{Wire meas., LOG formula} \end{cases} \qquad (14)$$

where we used $\eta = 0.243$.

6 DISCUSSION

The application of three different methods for kicker impedance evaluation has led to a fruitful criticism on the range of validity for these three techniques. We have seen indication for the limits of validity of the "classical" formula for a distributed impedance from coaxial wire measurements. The presence of the "hot" and "cold" conductor of a kicker is very important for the choice of the proper model geometry. The computer code HFSS was pushed beyond its usual range of application and has been modified for beam simulation (not only computer based coaxial wire method). As a further cross-check the heating of the kicker "in situ" caused by the SPS beam was measured and the temperature change has been calibrated in the laboratory in terms of a known heat deposition.

7 CONCLUSION

Temperature measurements have been made in the SPS to determine the heat generated by the beam in the ferrite of the kicker magnets. These measurements were made three hours after a beam stop during a short intervention on the outside of the kicker vacuum tanks and are preliminary. Final measurements on magnets equipped with RF-screened temperature monitors will be made after the shutdown. The temperatures measured on the vacuum tanks were calibrated in the laboratory to the temperatures and the heat deposition on the ferrite.

For a beam intensity of 1.9×10^{13} and 14.4 sec machine cycle, the temperature increase on the ferrite of the fast extraction kickers (MKE) is about 22°C, corresponding to a heat deposition of about 60 W.

On all other kicker magnets the temperature increase is negligibly small, probably due to the fact that, compared to the MKE magnets, these kickers have a larger vertical aperture, with the ferrite being further away from the beam.

The MKE measurements allow to extrapolate that the Curie temperature of 125°C (the temperature at which the magnetic properties of the ferrite are lost) will be reached at a beam intensity of about 4.7×10^{13} for a 14.4 sec machine cycle and at about 3×10^{13} for a 6 sec cycle.

The magnets will therefore be upgraded by a water cooling circuit, incorporated in the current conductor and touching the ferrite. This straightforward and not too costly measure will solve the heating problem for intensities above 5×10^{13} in a 6 sec cycle.

However it remains to be seen if the results of the measurements of the imaginary part of the beam impedance are tolerable from the beam point of view. A costly redesign of the MKE magnets would otherwise be required.

8 ACKNOWLEDGEMENTS

The results shown in this paper are the result of team work. This team consists of D. Brandt, M. D'yachkov, F. Ruggiero, G. Schröder, E.Shaposhnikova, H. Tsutsui, L.Vos and the author. In addition the helpful comments and suggestions by T. Linnecar as well as the support by R. Garoby are highly appreciated.

9 REFERENCES

[1] H. Tsutsui, "Some Simplified Models of Ferrite Kicker Magnet for Calculation of Longitudinal Coupling Impedance", CERN-SL-2000-004 AP, (2000).

[2] F. Caspers et al., "RF Screening by Thin Resistive Layers", Proceedings of the 1999 Particle Accelerator Conference, New York, 1408 (1999).

[3] H. Hahn and F. Pedersen, "On Coaxial Wire Measurements of the Longitudinal Coupling Impedance", BNL 50870, UC-28, Particle Accelerators and High Voltage Machines - TID-4500, (1978).

[4] H. Hahn, M. Morvillo, A. Ratti, "The Coupling Impedance of the RHIC Injection Kicker", AD/RHIC/RD-95, (1995).

[5] E. Jensen, “An Improved Log-formula for Homogeneously Distributed Impedance”, PS/RF/Note 2000-001, (2000).

[6] F. Caspers et al., “Impedance Measurement of the SPS MKE Kicker by Means of the Coaxial Wire Method”, PS/RF/Note 2000-004, (2000).

[7] L.S.Walling et al, “Transmission Line Impedance Measurements for an Advance Hadron Facility”, NIM, A **281**, 433 (1989).

[8] V.Vaccaro, “Coupling Impedance Measurements: an Improved Wire Method”, INFN/TC-94/023, (1994).

[9] See World Wide Web address http://www.ansoft.com

[10] W. Hartung et al., “Assessment of the Coupling Impedance of Beam Line Higher-Order Mode Loads”, Proceedings of the Workshop on Microwave-Absorbing Materials for Accelerators, (1993).

[11] T.Bohl, T.Linnecar, E.Shaposhnikova, “Emittance Control by the Modification of the Voltage Programme”, CERN SL-MD Note 246, (1997).

[12] G. Schröder, private communication.